Analysis of pre- and post-scission neutrons emitted in the reaction ^{169}Tm(^{36}Ar,f) at $E_{lab}=205$ MeV

H. Rossner, D. Hilscher, D. J. Hinde, B. Gebauer, M. Lehmann, and M. Wilpert
Hahn-Meitner-Institut Berlin, D-1000 Berlin 39, Federal Republic of Germany

E. Mordhorst
Universität Hamburg, D-2000 Hamburg 50, Federal Republic of Germany
(Received 31 May 1989)

Pre- and post-scission neutron multiplicities for the reaction ^{169}Tm(^{36}Ar,f) at $E_{lab}=205$ MeV were measured in coincidence with fission fragments of different masses and total kinetic energies. The mass and total kinetic energy dependence of the total neutron multiplicity as well as the width of the out-of-plane fission fragment correlation angle are well described by evaporation calculations. An average time before scission of several 10^{-20} s is deduced from the average pre-scission neutron multiplicity. The mass dependence of the post-scission neutron multiplicity is consistent with an energy division at scission proportional to the mass of the fragments. For the first time clear evidence for an increase in pre-scission neutrons with increasing total kinetic energy values has been observed. Possible interpretations of this unexpected behavior are discussed.

I. INTRODUCTION

Formation of a compound nucleus demands the equilibration of all nuclear degrees of freedom, and a subsequent division of the nucleus into two heavy fragments again implies a complicated rearrangement of nuclear matter. The displacement of nucleons in nuclei is less vigorous for less violent collisions and the amount of reorganization of nuclear degrees of freedom may be expressed by nuclear interaction times. In fact, it has been shown[1-4] that large-scale collective nuclear motion takes place on time scales which are longer by one to two orders of magnitude than the time scales for relaxation of single-particle degrees of freedom. For instance, for strongly damped collisions in the reaction ^{166}Er+^{86}Kr ($E/A=8.18$ MeV) relaxation times for the dissipation of radial kinetic energy (τ_R), the relative angular momentum (τ_l), and for the development of small-scale deformations (τ_α) were estimated to be $\tau_R=0.3\times10^{-21}$ s, $\tau_l=1.5\times10^{-21}$ s, and $\tau_\alpha=5\times10^{-21}$ s.[5] Interaction times of $(1-2.5)\times10^{-21}$ s were determined[6] for deeply inelastic reactions of the system ^{197}Au+^{238}U ($E/A=8.65$ MeV) (Ref. 7) analyzed within an energy-loss window of 100–350 MeV using the surface friction model. The mass equilibration process has been studied in fissionlike reactions[8] and it has been found that the mass drift toward symmetry has the characteristics of a strongly damped motion and occurs on a time scale of $t=(2-10)\times10^{-21}$ s. A theoretical investigation of the tilting mode of the dinuclear system ^{165}Ho+^{165}Ho (Ref. 9) demonstrated that relaxation times for the projection K of the total angular momentum I onto the symmetry axis strongly depend on the magnitude of I and can be longer than 10^{-20} s for $I<100\hbar$, indicating long time scales for fusion-fission reactions.

Measurements of pre- and post-scission neutron multiplicities provide a tool to compare fission time scales with neutron evaporation times. These times, though model dependent, may be used to clarify the definition of "normal" and "fast" fission processes, and further on may furnish conditions for the study of nuclear viscosity.[2-4] Recent systematic studies[2] of pre- and post-scission neutron multiplicities from heavy-ion-induced fusion-fission reactions, spanning a fissility range from 0.60 to 0.84, indicate that fission decay times are of the order of 10^{-20}–10^{-19} s and seem to be roughly independent of fissibility. For systems with no barrier for fission, a reduction in time scale up to a factor of 4 was observed. Further, it has been shown[1] that fission decay times are only weakly dependent on the excitation energy of the composite system, because a large part of the initial excitation energy is quickly carried away by pre-scission particle emission, such that the system close to scission is left with moderate excitation energy of roughly 60 MeV only.

In this work we studied the fission reaction ^{169}Tm(^{36}Ar,f) at $E_{lab}=205$ MeV. The compound nucleus ^{205}Fr formed in a complete fusion reaction has a fissility of $x=0.75$ and a rotating-liquid-drop fission barrier height[10] of $B_f=6.4$ MeV for zero spin; this barrier disappears for angular momenta larger than $69\hbar$. The fusion cross section of this reaction has been measured[11] as $\sigma_f=(660\pm100)$ mb, and the average spin value $\langle I\rangle$ was determined to be $48\hbar$, resulting in an average fission barrier height of 2 MeV. Calculations and systematics[12] showed that the probability for fission is high enough compared to particle evaporation such that the evaporation residue correction in the spin-dependent fission decay width could be neglected. From the mean fissility value[13] of $x_m=0.69$, one may conclude that extra-extra push effects or quasifission reactions have only minor influence on the reaction mechanism. Some contributions from noncompound fission,[14] however, may be expected because of the rather low average fission barrier

height, which is comparable to the nuclear temperature of the compound nucleus. From the neutron-deficient compound nucleus ^{205}Fr very few neutrons should be emitted before scission. Thus, fission fragment excitation energies and post-scission neutron multiplicities might be higher than in usual heavy-ion-induced fusion-fission reactions provided that the fission decay time is not changed drastically. A large ratio of post-scission to pre-scission neutrons certainly favors the study of characteristic features of fission fragments, such as excitation energy, temperature, and level-density parameter which, for example, can be determined from the post-scission neutron multiplicity, the slope of neutron energy spectra, and the width of the out-of-plane fragment correlation angle, respectively. The deduction of pre-scission neutrons for fission channels with different mass splits and total kinetic energies (TKE) further provides additional information about the fission process.

In Sec. II the experimental setup and procedure is described and in Sec. III we outline the features of the evaporation code used in the interpretation of the measured neutron multiplicities. Also the shape of the neutron-energy spectra used in the multiple-source fitting procedure is discussed and the neglect of neutrons being emitted during the acceleration phase of the fragments is justified. In Sec. IV the measurements of the out-of-plane fragment angular correlation, the mass-TKE correlation, and the number of neutrons detected in coincidence with fission fragments of different masses and TKE values are presented and compared with statistical model predictions. Our results are summarized in Sec. V.

II. EXPERIMENTAL PROCEDURE

A self-supporting 395-μg/cm^2-thick target of metallic ^{169}Tm was bombarded by a 205-MeV beam of ^{36}Ar from the VICKSI accelerator at the Hahn-Meitner-Institut. Kinematic coincidences between reaction products were detected by two position-sensitive low-pressure multiwire proportional chambers (MWPC). These detectors measured the in-plane and out-of-plane position of two heavy reaction products in addition to their times of flight, with respect to the cyclotron radio frequency (rf), and thus determined the fragment velocity vectors v_1 and v_2 in the laboratory system. For binary fission reactions conservation of linear momenta parallel ($m_1 v_1^{\parallel} + m_2 v_2^{\parallel} = A v_0$) and perpendicular ($m_1 v_1^{\perp} = m_2 v_2^{\perp}$) to the beam direction yields the velocity $v_0 = (v_1^{\perp} v_2^{\parallel} + v_2^{\perp} v_1^{\parallel})/(v_1^{\perp} + v_2^{\perp})$ of the center-of-mass (c.m.) system and the primary fragment masses m_1 and m_2 before post-scission particle evaporation assuming that m_1 and m_2 add up to the total mass A of the composite system. The total kinetic energy of the two fragments in the exit channel was calculated using their primary masses (m_1, m_2) and the deduced c.m. velocities.

The MWPC detectors were of different sizes: the larger one was a fourfold segmented type with a sensitive area of 244×122 mm^2, while the smaller one had just one segment with an area of 61×61 mm^2.[15] Both detectors were built of three parallel electrodes separated by 3 mm, a central cathode plane from which the time signal was derived, and two outer electrodes with an orthogonal grid structure with a wire gap of 1 mm for position measurements. The wires are connected to a high bandwidth delay line with 1 ns delay per tap.

The distance between the center of the sensitive cathode area and the target position was 284 mm for the larger chamber and 201 mm for the smaller one. The large MWPC detector was placed with its center at an in-plane angle of 98.5° with an angular acceptance of 45° in plane and ±11° out of plane. The other detector was positioned with its center at an in-plane angle of −42° and had an angular acceptance of 16° in plane and ±8° out of plane. Angle-calibrated slit masks were used for angle calibration. The mask for the larger detector was of cylindrical shape with a radius of 243.5 mm, and the in-plane angle positions were defined by 49 vertical slits with width of 0.3 mm separated by 4.25 mm from each other. The out-of-plane angle position was defined by 26 horizontal slits of the same width and separation. The mask for the smaller detector had 17 vertical and ten horizontal slits with width of 0.5 mm and again a separation of 4.25 mm in between. Both masks were placed on moveable arms within the scattering chamber and were moved to 0° and 180° for slit calibration using a telescope aligned along the beam line. Before and after the run the arms were precisely located in front of the MWPC detectors for angle calibration.

Two Ne102A plastic-scintillator detectors placed at 0° in plane and at 8° above and 7° below the reaction plane were used to monitor the vertical beam position and the time of flight of elastically scattered particles measured with respect to the cyclotron rf. The horizontal position of the beam was controlled by elastically scattered events detected in the MWPC detectors. The mass and TKE resolution for fission fragments in such a measurement may be strongly influenced by multiple scattering in the target. Therefore the half-width scattering angle $\delta_{1/2}$ for multiple scattering of an initially parallel beam of particles with charge Z_1 and center-of-mass energy $E_{\text{c.m.}}$ penetrating a material layer of charge Z_2 and thickness d has been calculated using the formula given by Meyer[16,17] as

$$\delta_{1/2} = \frac{2 Z_1 Z_2 e^2}{a_s E_{\text{c.m.}}} \left[g_1(\tau) + \frac{a_s^2}{r_0^2} g_2(\tau) \right] . \tag{1}$$

The scattering region is characterized by a sphere of radius r_0 with N atoms per unit volume and r_0 is set equal to half the distance of immediately neighboring atoms: $r_0 = 0.5 N^{-1/3}$. The screening of the nuclear charges by electronic shells is described by the parameter a_s which is given by $a_s = 0.468 (Z_1^{2/3} + Z_2^{2/3})^{-1/2} \times 10^{-8}$ cm. In Ref. 16 the functions $g_1(\tau)$ and $g_2(\tau)$ are tabulated for different values of the reduced target thickness $\tau = \pi a_s^2 N d$.

For fission fragments with half the compound nucleus mass and charge, the angle $\delta_{1/2}$ is plotted in Fig. 1 versus the detection angle θ. Kinetic energies at different values of θ were calculated from kinematics assuming the total kinetic energy to be given by systematics.[18] The ^{169}Tm layer thickness was assumed to be half the target thick-

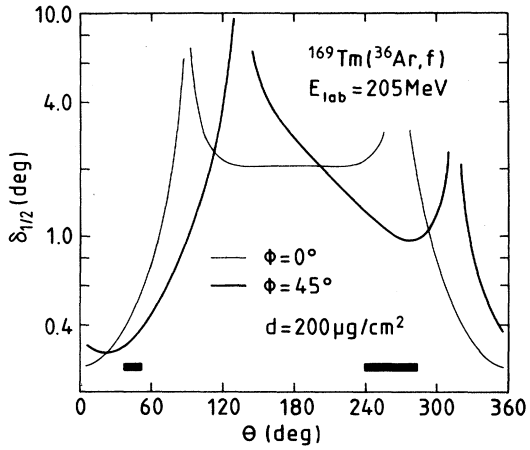

FIG. 1. Calculated multiple-angle scattering in a target foil of 200 $\mu g/cm^2$ thickness for symmetric fission fragments of the reaction $^{169}Tm(^{36}Ar,f)$ at $E_{lab}=205$ MeV. The dependence of the multiple-scattering half-width angle $\delta_{1/2}$ on the detection angle θ is shown for two target rotation angles of $\Phi=0°$ and $\Phi=45°$.

ness used in the experiment. Results for $\delta_{1/2}$ are shown for two angles of the target normal direction with respect to the beam direction: $\Phi_1=0°$ and $\Phi_2=45°$. The two horizontal bars in Fig. 1 indicate the angle regions covered by the multiwire detectors. For these detector positions obviously a target rotation angle of $\Phi=45°$ is favorable compared to $\Phi=0°$ and a half-width scattering angle of $\delta_{1/2}\approx 0.35°$ and $\delta_{1/2}\approx 1°$ is predicted for symmetric mass splits detected at $\theta\approx 42°$ and $\theta\approx 270°$, respectively.

An assumed systematic uncertainty in the angle calibration of the MWPC detectors of 0.5° yields an uncertainty in mass and total kinetic energy of 0.5 mass units and 0.5 MeV for symmetric fission fragments. Additional uncertainties are caused by the finite time resolution of the fragment detectors and the time spread of the beam bunches. For elastic scattering events, a full width at half-maximum (FWHM) value of $\Delta t\approx 0.7$ ns for the time of flight relative to the cyclotron rf was measured in both MWPC chambers. An estimated upper limit of $\Delta t_s\approx 0.5$ ns for the systematic error in time causes respective shifts of 1 mass unit and 8 MeV. So, the experimental uncertainties in angle and time yield absolute uncertainties in mass and TKE of symmetric fission fragments of 1.2 mass units and 8 MeV, respectively.

Seven neutron detectors consisting of liquid-scintillator cells (NE213 or BC501) optically coupled to photomultiplier tubes (XP 2041) were positioned outside the 3-mm-thick stainless-steel scattering chamber. Pulse shape and time-of-flight techniques were utilized to discriminate between γ rays and neutrons and to measure the neutron-energy spectra. Sizes and positions of these detectors are given in Table I.

Using the time-of-flight method the neutron-energy resolution was determined by the spread of the distance

TABLE I. Geometrical arrangement of the neutron detectors. In-plane angle θ_n, out-of-plane angle φ_n, and distance l refer to the center of the liquid-scintillator cell with respect to the target position. The liquid-scintillator cells were of cylindrical shape with diameter d and length b.

Detector no.	d (cm)	b (cm)	θ_n (deg)	φ_n (deg)	l (cm)
1	25.4	5.08	−90	0	186.0
2	25.4	10.16	−24	0	178.6
3	25.4	10.16	19	0	181.6
4	25.4	5.08	0	90	112.5
5	12.7	5.08	165	0	85.3
6	12.7	5.08	−165	0	84.5
7	12.7	5.08	−165	17	86.0

traveled by the neutron before being detected and by the time resolution achieved in the experiment. The uncertainty in the flight distance was set equal to the length b of the scintillator cells and the time spread of γ rays was measured to be ≈ 1.6 ns for all detectors throughout the experiment. At neutron energies of 1 MeV our energy resolution is dominated by the uncertainty in the flight distance and amounts to 6–13 %, whereas at neutron energies of 10 MeV our energy resolution is 9–20 % and is mostly due to the finite time resolution. The neutron detector efficiency was computed with a Monte Carlo code[19] for the specific neutron-energy threshold of 0.6 MeV used in the experiment, and the energy signals of the detectors were calibrated by standard γ sources (^{22}Na, ^{133}Ba, ^{241}Am). The calculated efficiencies have been checked by comparison with the neutron spectra measured with a ^{252}Cf source enclosed in a proportional gas counter with a solid angle close to 2π for the detection of fission fragments. From this comparison a systematic uncertainty of 8% is inferred for the neutron detection efficiency for energies larger than 1.5 MeV.

III. DATA ANALYSIS

A. Evaporation code

To compare the measured neutron multiplicities and energy spectra shapes with statistical-model predictions and to compute neutron evaporation times, a modified version of the evaporation code JULIAN (Ref. 20) was used. Another version of this code has been described by Gavron.[21] Here we outline our version and the basic assumptions used in our computations.

The statistical model defines the average lifetime τ of a compound nucleus at excitation energy E^* and spin I by its total decay width Γ,[22,23]

$$\hbar/\tau(E^*,I)=\Gamma(E^*,I)=\sum_i \Gamma_i(E^*,I)\ , \tag{2}$$

where Γ is the sum of partial widths Γ_i for all possible decay channels i. Applying the reciprocity theorem it has been shown[23] that the probabilities for formation and decay of a compound nucleus through channel i are related by $\Gamma_i\propto\epsilon_i\sigma_i$, where σ_i is the cross section for forma-

tion of the compound nucleus through channel i with channel energy ϵ_i. When individual initial and final states in the compound nucleus are not resolved, then the formation and decay probabilities within a given energy interval are weighted with their corresponding phase-space factors. In that case the partial decay width $\Gamma_i(E^*,I)$ is usually expressed by level densities ρ of the initial and final nuclei and by transmission coefficients T_l

$$\Gamma_i(E^*,I)=\frac{(2s_i+1)}{2\pi\rho(E^*,I)}\sum_{l=0}^{\infty}\sum_{J=|I-l|}^{J=|I+l|}\int_0^{E^*-B_i}\rho(E^*-B_i-\epsilon_i,J)T_l(\epsilon_i)d\epsilon_i \ . \tag{3}$$

Here J and $E_f^*=E^*-B_i-\epsilon_i$ are the spin and total excitation energy of the final nucleus, when a particle with spin s_i and kinetic energy ϵ_i is emitted from an initial nucleus with spin I and total excitation energy E^*, while B_i and l denote the binding energy and the orbital angular momentum of the emitted particle. The spin-dependent level density $\rho(E_f^*,J)$ of the final nucleus is calculated by the difference of state densities[24–26] $\rho(E_f^*,J)=\omega(E_f^*,M=J)-\omega(E_f^*,M=J+1)$, and the density of all states at excitation energy E_f^* and with projection M of the nuclear spin vector along some arbitrary quantization axis is defined by $\omega(E_f^*,M)=\omega([E_f^*-M^2/aR\,],0)$, where a is the level-density parameter and R is related to the effective moment of inertia $\mathcal{T}$ of the nucleus by $aR\hbar=2\mathcal{T}$.

The decay paths are followed using a Monte Carlo technique. The calculation starts with the excited compound nucleus and proceeds until the end of the evaporation cascade is reached or until fission occurs. This method allows the practical calculation of yields, energy spectra, and angular distributions of emitted particles and of heavy residual nuclei. As discussed below, the lifetime of the compound nucleus for particle emission can also be extracted easily. Evaporation of γ rays, n, p, d, t, ^{3}He, α, ^{6}Li, and ^{7}Li can be handled by the code in addition to the fission decay. Transmission coefficients for particle emission are computed by a complete optical-model (OM) routine incorporated in the program. In the computations described in this paper the evaporation of n, p, d, and α particles were taken into account with OM parameters given by Wilmore and Hodgson,[27] Perey,[28] Lohr and Haeberli,[29] and Huizenga and Igo,[30] respectively. Fission decay widths were calculated with the assumption of equal level-density parameters for transition state and compound nucleus ($a_f/a_n=1$) and by use of the spin-dependent fission barriers of the finite-range rotating-liquid-drop model.[10]

For each decay step the average lifetime τ of the nucleus is defined by $\tau=\hbar/\Gamma$. In order to get an actual decay time t_d in the Monte Carlo procedure applied here, τ is multiplied by the negative logarithm of a random number R chosen in the interval between 0 and 1 (Ref. 3)

$$t_d=-\tau\ln R \ . \tag{4}$$

Individual spectra of decay times accumulated from 20 000 cascades, starting with the compound nucleus ^{205}Fr at an initial excitation energy of $E^*=77$ MeV, are shown in Fig. 2 for the first three evaporated neutrons. In each decay step these times are spread around the specific average decay time τ and will be increased by the decrease of thermal excitation energy due to rotational energy or charged-particle emission before neutron evaporation. Each value on the time axis in Fig. 2 represents a certain lifetime of the compound nucleus and will define a certain distribution of the neutron multiplicity M_n. The dependence of $\langle M_n \rangle$ on the lifetime is shown in Fig. 3 for the level-density parameter $a=A/8$ MeV^{-1} and $a=A/10$ MeV.$^{-1}$. This dependence is used to associate a fission decay time to the number of pre-scission neutrons. No attempts have been made to include deformation effects or to distinguish between neutrons that are emitted during the time needed to pass the saddle configuration and those neutrons that are emitted on the path of the nucleus to the scission configuration.[2,3] The fission time scale defined above is meant to provide a simple tool for measuring the speed of fission relative to the speed of neutron evaporation from spherical compound nuclei. This time scale does not take into consideration the increase in thermal excitation energy for fissile systems passing from the equilibrium configuration to the scission configuration. The respective portions of this energy available for pre- and post-scission particle evaporation will depend on the fission dynamics, and a recent

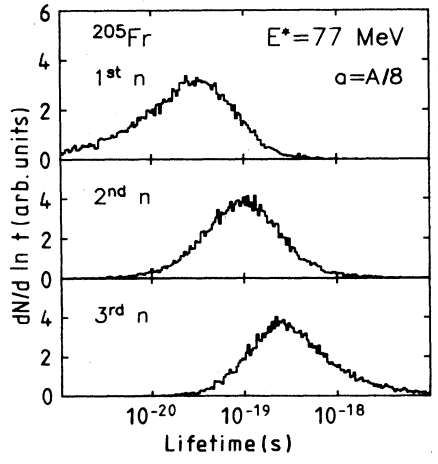

FIG. 2. Computed spectra of compound nucleus decay times for the first, the second, and the third neutron emitted from the initial nucleus ^{205}Fr at an excitation energy of $E^*=77$ MeV. A level-density parameter of $a=A/8$ MeV^{-1} was assumed in these evaporation calculations.

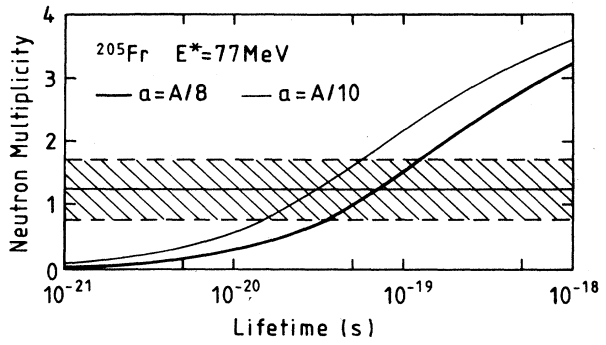

FIG. 3. Relation between average neutron number and lifetime of the compound nucleus ^{205}Fr at $E^*=77$ MeV. The relation is shown for a level-density parameter of $a=A/8$ MeV^{-1} (thin line) and $a=A/10$ MeV^{-1} (thick line).

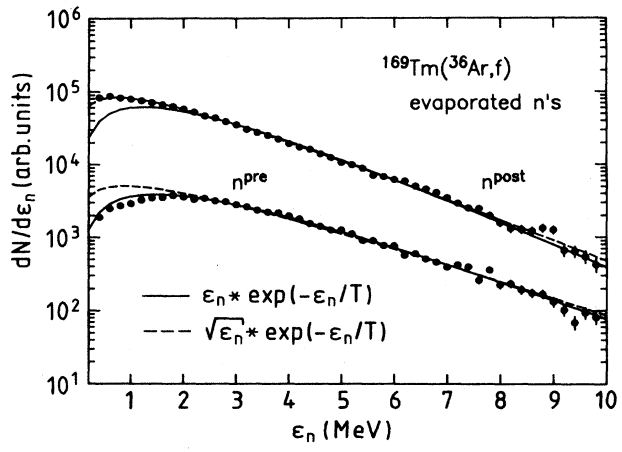

FIG. 4. Computed energy spectra of pre- and post-scission neutrons. The results of an evaporation code (dots) are compared with energy spectra shape parametrizations for a Maxwellian distribution (solid line) and a Watt distribution (dashed line).

compilation of post-scission neutron multiplicities[31] indicates that a considerable part of this energy is stored in the fragments.

B. Shape of neutron spectra

Usually the energy distribution $P(\epsilon_n)$ of neutrons being evaporated with kinetic energy ϵ_n is parametrized as

$$P(\epsilon_n) \propto \epsilon_n^k \exp\left[-\frac{\epsilon_n}{T}\right] . \tag{5}$$

The parameter T represents the nuclear temperature of the residual nucleus and $k=1$ for a Maxwellian distribution. For neutrons emitted during a neutron evaporation cascade the energy spectrum can also be described by the equation above using $k=\frac{5}{11}$,[32] and it has been demonstrated that even the spectrum shape of post-scission neutrons, which are ejected from different nuclei with different excitation energies, can be reproduced very well with $k\approx\frac{1}{2}$.[33,34]

In Fig. 4 the two different shapes given by Eq. (5) when $k=1$ and $k=\frac{1}{2}$ are compared with pre- and post-scission neutron-energy spectra generated by evaporation calculations using Fermi-gas level densities with a level-density parameter $a=A/8$ MeV^{-1}. The computations are performed for the compound nucleus ^{205}Fr with total excitation energy $E^*=77$ MeV and a spin distribution based on transmission coefficients calculated with the Bass potential.[35] The minimum lifetime of the compound nucleus before fission has been adjusted in the evaporation code to reproduce the measured pre-scission neutron multiplicity. In Fig. 4 it is demonstrated that the spectrum shape of pre-scission neutrons with multiplicity $M_n^{pre}=1.25$ (lower part), in fact, is similar to a Maxwellian distribution ($k=1$) and that the spectrum shape of post-scission neutrons with multiplicity $M_{n,F}^{post}=3.5$ (upper part) is reproduced very well by a Watt distribution ($k=\frac{1}{2}$).

The two neutron-energy spectra parametrizations shown in Fig. 4 are used in the multiple-source least-squares fitting procedure to extract multiplicities $M_n^{pre,post}$ and temperature parameters $T^{pre,post}$ of pre- and post-scission neutrons from the measured spectra. Three moving sources were considered: the compound nucleus formed in a complete fusion reaction and the two correlated fission fragments after full acceleration. It was assumed that the neutrons are emitted isotropically[4] in their respective rest frame. Thus, the measured double-differential neutron multiplicities were formally decomposed into three terms,[36]

$$\frac{d^2M_n}{d\epsilon_n d\Omega_n} = \frac{M_n^{pre}\epsilon_n}{4\pi(T^{pre})^2}\exp\left[-\frac{\epsilon_n - 2\sqrt{\epsilon_n\epsilon_C/A_C}\cos\Psi_C + \epsilon_C/A_C}{T^{pre}}\right] + \sum_{i=1}^{2}\frac{M_{n,i}^{post}\sqrt{\epsilon_n}}{2(\pi T^{post})^{3/2}}\exp\left[-\frac{\epsilon_n - 2\sqrt{\epsilon_n\epsilon_i/A_i}\cos\Psi_i + \epsilon_i/A_i}{T^{post}}\right] . \tag{6}$$

Measured average values for the recoil energy ϵ_C of the compound nucleus and for the kinetic energies ϵ_i of the fission fragments have been used. These values agreed within 3% with kinetic energies calculated from systematics.[18] For the relative angles Ψ_C and Ψ_i between neutron direction and source direction, the angular acceptance of the neutron detector and the width of the experimental acceptance angle of the fission fragments were

taken into account in the fitting procedure. Double-differential neutron multiplicities of the seven detectors measured in coincidence with symmetric fission fragments are plotted in Fig. 5 for the energy interval between 0 and 10 MeV and a bin size of 0.1 MeV. The decomposition of these spectra in pre- and post-scission components achieved by the multiple-source fitting procedure is displayed by solid and structured lines. The dot-dashed line, the dashed line, the dotted line, and the solid line represent the pre-scission component, the two post-scission components of the correlated fragments, and the sum of all components, respectively. It should be stressed that the assumption of isotropic neutron emission in the rest frame of the emitters results in a very good reproduction of the measured out-of-plane neutron yield at $\theta_n = 0°$, $\varphi_n = 90°$ for all fission fragment mass and TKE cuts described in Sec. IV C. We therefore conclude that within errors, anisotropic neutron emission is negligible in the reaction studied here, in agreement with former investigations of a similar system ^{141}Pr+^{40}Ar (316 MeV) (Ref. 4) and other projectile-target combinations,[4,37] where the in-plane as well as the out-of-plane neutron yield was measured. In Fig. 6 the differential multiplicities resulting from an integration of the energy spectra between 2 and 5 MeV are shown for the measured in-plane neutron detector angles and compared with the results of the multiple-source fit. The neutron yields in the out-of-plane detector positioned at $\theta_n = 0°$ and $\varphi_n = 90°$ are plotted as squares at the two in-plane angles of $\theta_n = -90°$ and $\theta_n = +90°$ and the yields in the two backward detectors at $\theta_n = -165°$, $\varphi_n = 0°$ and $\theta_n = -165°$, $\varphi_n = 17°$ have been averaged. In this figure the same line structure as the one used in Fig. 5 is applied for the representation of the different neutron sources.

TABLE II. Comparison of experimentally deduced T_{exp} and calculated T_{calc} temperature parameters of pre- and post-scission neutron-energy spectra generated in the reaction ^{205}Tm(^{36}Ar,f) at $E_{lab} = 205$ MeV.

		$a = A/8$ MeV^{-1}	$a = A/10$ MeV^{-1}
	T_{exp} (MeV)	T_{calc} (MeV)	T_{calc} (MeV)
n^{pre}	1.27±0.35	1.43	1.57
n^{post}	1.42±0.07	1.46	1.62

Values for T_{exp} deduced from the slope of the measured neutron energy spectra for fission fragments averaged over mass and total kinetic energy are compared in Table II with parameters T_{calc} deduced from computed spectra using two different level-density parameters of $a = A/8$ MeV^{-1} and $a = A/10$ MeV^{-1}. The very similarity of T_{calc} for pre- and post-scission neutrons indicates that the positive fission Q values of this system on the average cause thermal excitation energies per nucleon

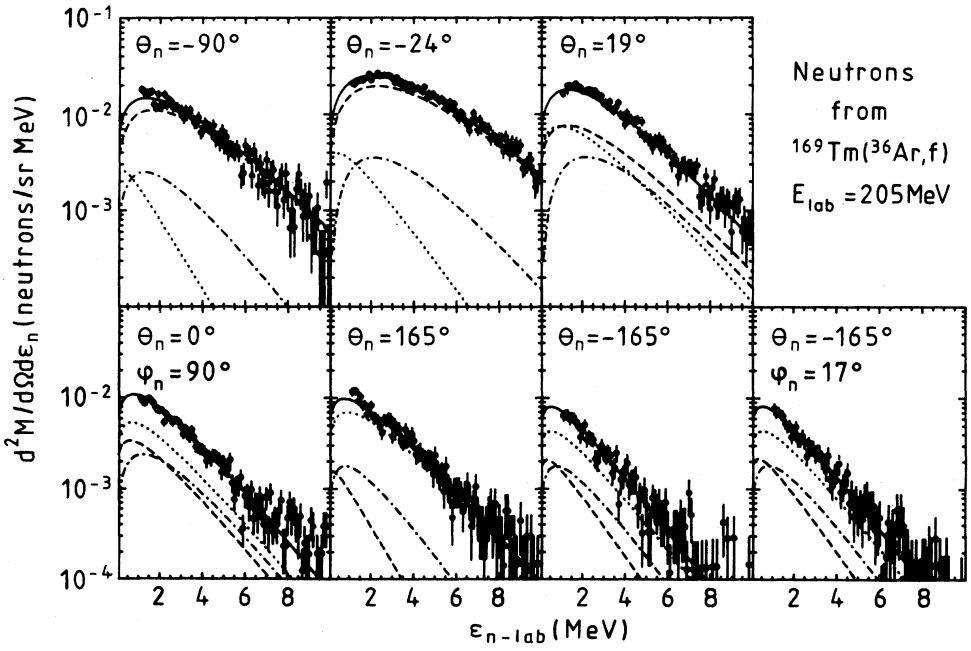

FIG. 5. Neutron-energy spectra measured at various angles in coincidence with symmetric fission fragments of the system ^{169}Tm+^{36}Ar (205 MeV), detected at mean scattering angles of $\langle\theta_{F_1}\rangle = -42.5°$ and $\langle\theta_{F_2}\rangle = 89.0°$. The results of a multiple-source fit are displayed by lines and represent the neutron yield contribution of the composite system before scission (dashed-dotted line) and of the two correlated fragments (dotted and dashed lines) after full acceleration.

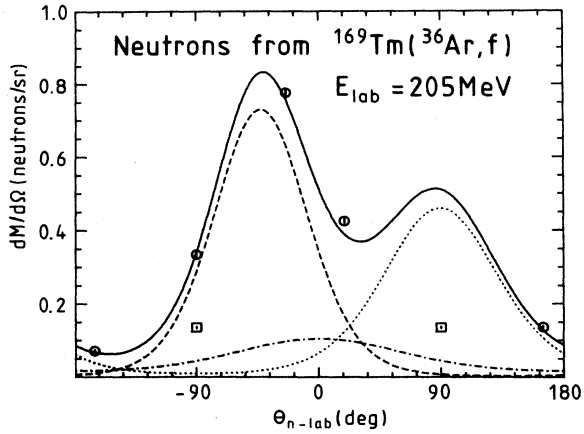

FIG. 6. Neutron yields deduced from the energy spectra shown in Fig. 5 by integration between 2 and 6 MeV. The detector positioned at $\theta_n = 0°$, $\varphi_n = 90°$ is displayed by squares at $\theta_n = -90°$ and $\theta_n = +90°$, and the yields of the two detectors at $\theta_n = -165°$ have been averaged.

of fission fragments ($E_F^*/A = 0.38$ MeV) to be roughly the same as those of the compound nucleus ($E_C^*/A = 0.37$ MeV) when spherical shapes are considered. Within errors the temperature parameter T_{exp} for post-scission neutrons is reproduced by $a = A/8$ MeV^{-1}, whereas the accuracy of T_{exp} for pre-scission neutrons is not sufficient to favor a certain level-density parameter. The uncertainties for T_{exp} given in Table II refer to an increase of 5% in the χ^2 value of the multiple-source fit. They do not include the systematic uncertainties discussed in Sec. II.

C. Acceleration neutrons

Usually it is assumed that post-scission neutrons are emitted by fully accelerated fragments. Measurements of neutron spectra at various angles with respect to the direction of flight of a fragment in the case of spontaneous fission (^{252}Cf) (Ref. 34) and in thermal neutron-induced fission[38] have verified this assumption. For fission at high excitation energies with shorter lifetimes for neutron emission, customarily the same assumption is applied in the analysis of neutron spectra. This supposition might be questionable.[39] We want to point out, however, that scission obviously occurs at moderate excitation energies only.[1] But, for the relatively neutron-poor composite system ^{205}Fr each symmetric fission fragment at scission is left at a relatively high excitation energy of roughly 40 MeV. According to evaporation calculations for spherical nuclei, this excitation energy yields a neutron multiplicity of $M_{n,F} = 0.2$ within a time interval of 10^{-20} s, which is distinctly larger than the time of 3×10^{-21} s needed to reach 80% of the final fragment velocity. These considerations indicate that even for fission fragments at relatively high excitation energy, neutron emission during fragment acceleration time should only give minor contributions to the pre-scission neutron multiplicity in agreement with earlier considerations.[37,40]

A rough estimate of the time scale for neutron emission can further be deduced from the angular correlation of neutrons with respect to the fragment direction. If the neutrons are emitted at times longer than the acceleration times of the fission fragments, the neutrons will appear at angles strongly correlated with the detection angles of the fission fragments. This, in fact, is observed experimentally in Fig. 6, and supports the assumption that most of the neutrons are mainly emitted from fully accelerated fragments.

IV. RESULTS AND DISCUSSION

A. Out-of-plane fragment angular correlation

The out-of-plane correlation angle spectrum for coincident fission fragments is shown in Fig. 7. Fitted with a Gaussian shape, the σ value of this distribution is $\sigma_\phi = 2.9°$. The main contribution to this width is expected to come from recoil effects due to evaporated particles (σ_{ev}). In addition to this recoil effect, multiple scattering (MS) of the fragments in the target foil increases the total variance σ_ϕ^2 of the out-of-plane angular correlation to

$$\sigma_\phi^2 = \sigma_{ev}^2 + \sigma_{MS,F_1}^2 + \sigma_{MS,F_2}^2 \ . \tag{7}$$

The multiple-scattering values σ_{MS,F_i} ($i = 1,2$) for symmetric fission fragments going in forward and more backward directions with respect to the beam direction are σ_{MS,F_1} ($\theta_{lab} = 42°$) $\approx 0.3°$ and σ_{MS,F_2} ($\theta_{lab} = 270°$) $\approx 0.85°$ (see Fig. 1). Analytical formulas for σ_{ev} were given in the literature[41] considering only neutron evaporation under two extreme cases where either all neutrons are emitted from the fully accelerated fragments or where all neutrons are emitted from the compound nucleus. To be more realistic, the width σ_{ev} due to pre- and post-scission particle emission was calculated by the evaporation code

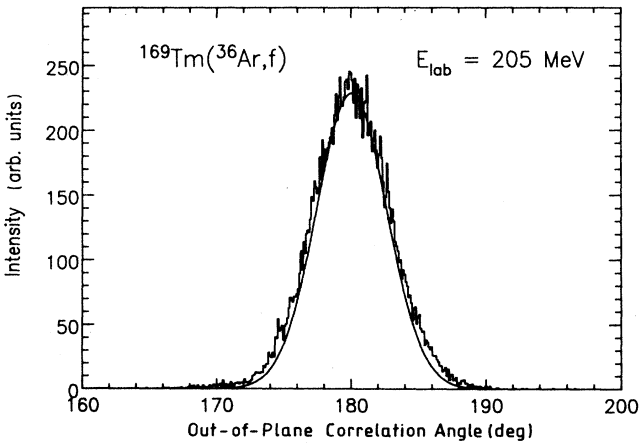

FIG. 7. Out-of-plane correlation angle of fission fragments produced in the reaction ^{169}Tm(^{36}Ar,f) at $E_{lab} = 205$ MeV. The Gaussian curve represents the result of an evaporation code assuming a level-density parameter of $a = A/10$ MeV^{-1} and pre- and post-scission neutron multiplicities as given in Table III.

using correlated symmetric fission fragments. It was assumed that the fragments are emitted in the reaction plane defined by the MWPC detectors into correlated scattering angles of $\theta_{c.m.}=60°/240°$ after evaporation of 1.25 pre-scission neutrons. The code followed the velocity vectors of composite system and fully accelerated fission fragments considering the change of the velocity vectors due to the recoil momentum of isotropically emitted particles (n,p,d,α). The calculated width of the out-of-plane correlation angle depends on the average kinetic energy of the evaporated particles and thus on the level-density parameter used in the computations. For $a=A/8$ MeV^{-1} ($a=A/10$ MeV^{-1}) we get $\sigma_{ev}^{pre}=1.39°$ ($\sigma_{ev}^{pre}=1.51°$) before and $\sigma_{ev}=2.23°$ ($\sigma_{ev}=2.5°$) including post-scission particle emission. The total calculated value is $\sigma_\phi=2.41°$ ($\sigma_\phi=2.61°$) and the Gaussian curve with $\sigma_\phi=2.61°$ is shown in Fig. 7. Referring to the discussion of T_{exp} in Sec. II, it seems that the present experimental accuracy of the neutron energy and the fission fragment correlation angle was not sufficient to determine a consistent level-density parameter from such a comparison.

B. Mass TKE correlation

The correlation between the total kinetic-energy distribution and the fragment mass is illustrated in Fig. 8. The two-dimensional contour lines in this figure represent lines of constant yield with a difference of 10% relative to the maximum yield for symmetric fission. Qualitatively, there is no dramatic dependence of the total kinetic-energy distribution on the mass asymmetry, which might be due to the large spread in the TKE distribution. This weak dependence of the most probable kinetic energy on the asymmetry of the mass split remains a characteristic feature also for the fusion-fission-like reactions occurring for heavier systems.[42] It has further been observed[42–44] that the spread in kinetic-energy release in heavy-ion-induced fission is only weakly dependent on excitation energy for fissilities $x<0.7$, whereas the width and the excitation energy dependence increases for $x>0.7$. These results were explained in terms of the change in equilibrium saddle shapes: at low spins and low fissility the saddle shape and the scission shape are nearly identical and thus the descent from saddle to scission might be too rapid to allow a significant deviation of the fragment properties from their values at the saddle point. In contrast, with increasing spin and fissility the saddle shape becomes more cylindrical in shape, and the nucleus may have more paths of different length to proceed to the scission configuration. Due to the strong dependence of the Coulomb energy on the separation distance between the fragments, a broadening of the total kinetic energy is expected.

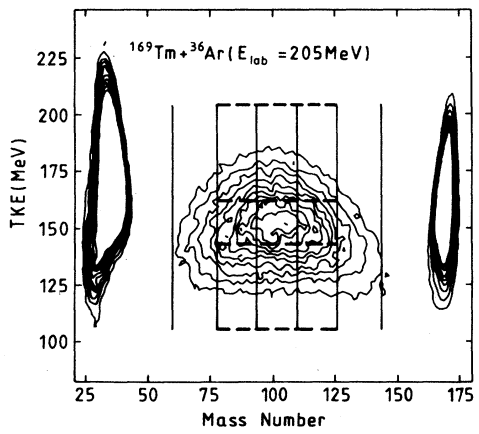

FIG. 8. Contour plot of the correlation between fragment mass and total kinetic energy (TKE). The contour lines represent a change of intensity in steps of 10% relative to the maximum yield of symmetric fission fragments. Mass and TKE bins, where the respective dependences of pre-scission, post-scission, and total neutron multiplicities were determined (see Figs. 9 and 11), are indicated by vertical solid lines and horizontal dashed lines.

The measured mean total kinetic energy of the fragments emitted in the fusion-fission reaction ^{169}Tm(^{36}Ar,f) at $E_{lab}=205$ MeV is TKE$=151\pm8$ MeV. Taking into account one pre-scission neutron ($A=204$) the TKE value is in slightly better agreement with the parametrization given in Refs. 45 and 46, TKE$=0.14Z_C^2/A^{1/3}-30=150.0$ MeV, than with the value predicted by a different systematic,[18] TKE$=0.1189Z_C^2/A^{1/3}+7.3=160.2$ MeV. When TKE is approximately expressed as a point-charge Coulomb energy between the two fragments such as TKE$=Z_{F_1}Z_{F_2}e^2/d$, the spread in TKE is related to the fluctuation in the distance d between the fragments at scission and from the measured value of $\sigma_{TKE}=13.9$ MeV we get $\sigma_d=1.7$ fm.

The measured mass width of $\sigma_A=18.7$ is consistent with values deduced from mass distributions of heavy-ion-induced fusion-fission reactions.[8,42] This spread cannot be explained by the statistical model, (SM), which predicts a width of $\sigma_A^{SM}=15.3$, when the probability for mass split A is defined by the thermal excitation energy $E_{th,sc}^*$ and the nuclear temperature T at scission by $P(A)\propto\exp\{E_{th,sc}^*(A)/T(A)\}$. The statistical model calculations for σ_A^{SM} were performed for a nuclear level-density parameter $a=A/10$ MeV^{-1} and an excitation energy defined by Eq. (8) in Sec. IV C.

C. Mass and TKE dependence of the neutron multiplicity

Neutron multiplicities measured in coincidence with fission fragments of different mass and TKE values were analyzed and discussed by several groups.[40,47,48] Hinde *et al.*[48] in particular showed that the gradient of the relation between post-scission neutron multiplicity per fragment and fragment mass $dM_{n,F}^{post}/dA$ is smaller for the heavy-ion-induced reaction ^{232}Th(^{19}F,f) than observed for spontaneous fission of ^{252}Cf. From this result one might expect a relatively low gradient for an Ar-induced fusion-fission reaction.

The specific regions of the fragment mass -TKE contour plot used in our analysis are indicated in Fig. 8 by vertical solid lines (mass) and horizontal dashed lines

(TKE). The multiple-source fit parameters for neutron multiplicity and nuclear temperature with minimum χ^2 values ranging from 0.9 to 1.5 are listed in Table III. The uncertainties shown in the table correspond to an increase of the minimum χ^2 value by 5%. For the mass bin fitting procedure the same fragment temperatures $T^{\text{post}}=T_{F_1}^{\text{post}}=T_{F_2}^{\text{post}}$ were used and for each mass bin the neutron multiplicities obtained for forward and backward emitted fragments were averaged. Roughly symmetric fragments occur in the TKE bins and therefore the same post-scission neutron multiplicities per fragment $M_{n,F_1}^{\text{post}}=M_{n,F_2}^{\text{post}}$ were assumed.

The values for total (filled circles), pre-scission (filled triangles), and post-scission (filled squares) neutron multiplicities extracted from the multiple-source fits are plotted in Figs. 9 and 11 as a function of mass and TKE, respectively, and are compared with results of evaporation calculations (small crosses). The computed post-scission neutron multiplicity per fragment has been determined from the thermal excitation energy $E_{\text{th,sc}}^{*}$ at scission. This excitation energy was calculated from the relation

$$E_{\text{th,sc}}^{*}=E_{\text{c.m.}}+Q_{FF}-TKE-E_{\text{rot}}(i_1,i_2)-E_{PP}\ , \quad (8)$$

where E_{PP} is the energy taken away by pre-scission particle emission (here particle evaporation) and $E_{\text{rot}}(i_1,i_2)$ is the rotational energy corresponding to the fragment spins i_1 and i_2. The thermal excitation energy at scission was split between spherical fragments in proportion to their mass. Experimental TKE values comprise the pre-scission kinetic energy, the rotational energy corresponding to the orbital angular momentum, and the Coulomb energy. Because the latter component is by far the largest one, the TKE values used in the calculation for different mass fragmentations were computed as point-charge Coulomb energies adjusted to the measured value for a symmetric mass split

$$\text{TKE}=\text{TKE}_{\text{sym}}^{\text{exp}}\frac{4Z_1Z_2}{Z_C^2}\frac{(4A_C)^{1/3}}{A_1^{1/3}+A_2^{1/3}}\ . \quad (9)$$

It was further assumed that the neutron-to-proton ratio of each fragment is equal to this ratio of the composite system after pre-scission particle evaporation. To compute $E_{\text{rot}}(i_1,i_2)$ the total spin I of the system at scission was decomposed into a component parallel to the scission axis (S_0) and a component perpendicular to the scission axis (l) with $I^2=l^2+S_0^2$. An average value for S_0 was calculated from the statistical scission model[49] and the components of the fragment spins i_1 and i_2 parallel and perpendicular to the scission axis were calculated from S_0 and l assuming a sticking condition between two spheres. The values for $E_{\text{rot}}(i_1,i_2)$ are of the order of a few MeV and thus, in fact, have only a minor influence on the post-scission neutron multiplicities.

Within errors the average number of pre-scission neutrons, displayed in Fig. 9 by filled triangles, is found to be

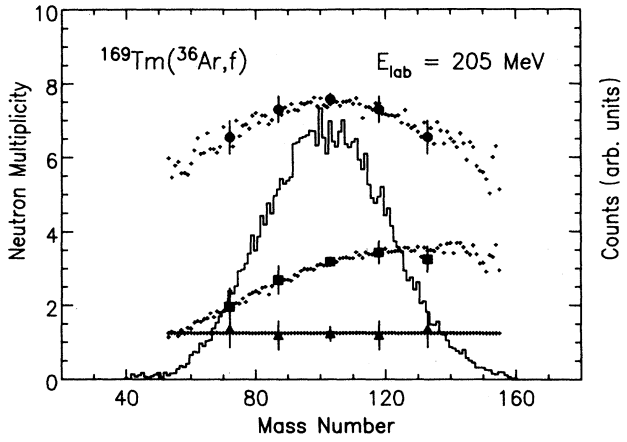

FIG. 9. Pre-scission (filled triangles), single-fragment post-scission (filled squares) and total neutron multiplicities (filled circles) measured for the fragment-mass bins shown in Fig. 8. Results of statistical model computations indicated by small crosses for the three specific neutron multiplicities demonstrate good agreement between experimental and calculated multiplicities. The histogram displays the experimental fragment-mass distribution.

TABLE III. Multiplicities M and temperature parameters T of pre- and post-scission neutrons extracted from the multiple-source fit. The post-scission neutron multiplicity M_n^{post} listed as a function of TKE is the sum of both fragment multiplicities: $M_n^{\text{post}}=M_{n,F_1}^{\text{post}}+M_{n,F_2}^{\text{post}}$.

$\langle A\rangle$	M_n^{pre}	T_m^{pre} (MeV)	$M_{n,F}^{\text{post}}$	T^{post} (MeV)
71.7	1.3±0.6	1.2±0.2	2.0±0.5	1.3±0.1
87.4	1.2±0.5	1.2±0.2	2.7±0.4	1.4±0.1
102.5	1.2±0.2	1.3±0.3	3.2±0.1	1.5±0.1
117.6	1.2±0.5	1.3±0.4	3.4±0.4	1.4±0.1
133.4	1.3±0.6	1.3±0.5	3.2±0.4	1.4±0.1
$\langle$TKE$\rangle$ (MeV)			M_n^{post}	
135.4	0.5±0.3	1.5±0.7	7.6±0.2	1.5±0.1
153.6	1.5±0.2	1.3±0.2	5.8±0.2	1.4±0.1
173.0	2.1±0.2	1.1±0.1	4.4±0.3	1.4±0.1

independent of the mass ratio. Interpretation of this pre-scission neutron multiplicity in terms of decay times of the compound nucleus yields times of $(70^{+55}_{-36})\times10^{-21}$ s $[(32^{+23}_{-17})\times10^{-21}$ s] for a level-density parameter of $a=A/8$ MeV^{-1} ($a=A/10$ MeV^{-1}) (see Fig. 3). An estimate for the lower limit of fission decay times may be deduced from the rigid-rotor rotational times when some assumptions are made about the shape of the rotating system. The observation of an angle-independent average mass of the fission fragments[11] indicates that at least one rotation of the composite system was completed before scission. With $\langle I\rangle=48\hbar$ (Ref. 11) and a radius parameter of $r_0=1.2249$ fm the times needed for one rotation are 8.8×10^{-21} s and 19.4×10^{-21} s for rigid-rotor shapes of a sphere and two touching spheres, respectively. The times extracted from the number of pre-scission neutrons exceed the minimum decay time deduced from the rigid-rotor model. However, according to the existing systematics of fission decay times[2] these times are roughly a factor of 2 shorter than expected for a fusion-fission reaction. So, even if components from noncompound fission reactions have not been observed in measurements of the fission fragment angular distribution and the angle dependence of the average fragment mass for the reaction ^{169}Tm(^{36}Ar,f) at $E_{\rm lab}=205$ MeV,[11] our results suggest that fission decay times deduced from pre-scission neutron multiplicities might be a very sensitive tool to study the onset of fast fission reactions.

The measured post-scission neutron multiplicity $M^{\rm post}_{n,F}$ for a fragment of mass A (solid squares in Fig. 9) displays a smooth dependence on fragment mass in agreement with measurements for compound nuclei of similar masses such as ^{209}Bi+p(155 MeV) (Ref. 40) and ^{209}Bi+α(45 MeV) (Ref. 47). However, our average gradient $dM^{\rm post}_{n,F}/dA$ with magnitude of ≈0.023 neutrons per mass unit is smaller than observed for the system ^{209}Bi+α with a slope of ≈0.039 neutrons per mass unit. A similar reduction of this gradient for heavy-ion-induced fusion-fission reactions was reported by Hinde *et al.*[48] Their post-scission neutron multiplicities measured for the system ^{19}F+^{232}Th exhibit an average gradient of ≈0.025 neutrons per mass unit, which is smaller by a factor of ≈3 than the gradient observed for ^{252}Cf and predicted by the random neck rupture (RNR) model.[50] Taking into account the evaporation of pre-scission particles, the fragment mass dependence of the post-scission neutrons can be reproduced by the statistical-model calculations described above. The comparison between fragment excitation energies E^*_F predicted by the statistical model (small crosses) and the RNR model (dots) is shown in the lower part of Fig. 10. Application of the evaporation code using these excitation energies then yields the post-scission neutron multiplicities $M^{\rm post}_{n,F}$ displayed in the upper part of Fig. 10. In the RNR model calculations one pre-scission neutron has been taken into account subtracting 12 MeV from the initial compound nucleus excitation energy. We further notice that the larger excitation energies of heavier fragments predicted by the RNR model, in fact, causes a larger neutron yield which is not degraded by charged-particle evaporation, even if, for instance, the ratio for proton to neutron

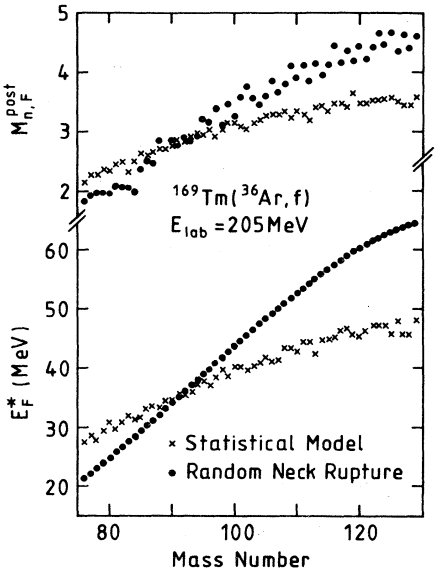

FIG. 10. Comparison of fragment-mass dependences for excitation energy and neutron multiplicity between the statistical model (small crosses) and the random neck rupture model (dots).

evaporation increases by a factor of 20 going from 2×10^{-3} at $A_F=75$ to 4×10^{-2} at $A_F=129$ according to evaporation calculations using spherical fragments. The fragment deformation effect of the RNR model, manifested in the larger slopes dE^*_F/dA_F and $dM^{\rm post}_{n,F}/dA_F$ is not observed in the measured post-scission neutron multiplicities. Comparison of measured (filled circles) and calculated (small crosses) total neutron multiplicities for individual mass bins (Fig. 9) indicates that the total thermal energy available for particle evaporation is described reasonably well by our statistical-model calculation.

Neutron multiplicities obtained from the multiple-source fit for different TKE bins are displayed in Fig. 11. As expected from energy conservation we observe within experimental uncertainties good agreement between measured and computed total neutron multiplicities, and the average gradient dTKE$/dM^{\rm post}_n$ has a value of 11.8 MeV which is similar to the value of ≈11.4 MeV for the system ^{209}Bi+α.[47] However, the observed dependence of the pre-scission neutron multiplicity on TKE is unexpected. Using the relation between the number of evaporated neutrons and the lifetime of the compound nucleus shown in Fig. 3 we get TKE-dependent fission decay times of 20×10^{-21} s (9×10^{-21} s), 95×10^{-21} s (44×10^{-21} s), 200×10^{-21} s (90×10^{-21} s) for TKE values of 135.4, 153.6, and 173.0 MeV, respectively, using a level-density parameter of $a=A/8$ MeV^{-1} ($a=A/10$ MeV^{-1}). If we remember that the low (high) TKE values originate from elongated (compact) scission shapes, then one might conclude that fission decay times increase with decreasing elongation of the composite system at scission. Assuming that in noncompound fission reactions less compact shapes are reached than in fusion-fission reac-

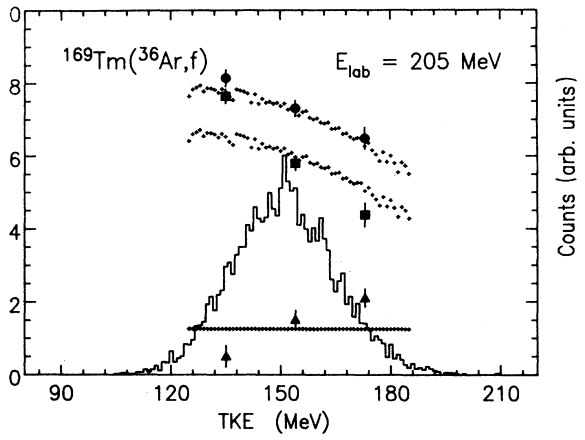

FIG. 11. Pre-scission (filled triangles), post-scission (filled squares), and total neutron multiplicities (filled circles) measured for the fragment total kinetic-energy (TKE) bins shown in Fig. 8. The histogram displays the experimental TKE distribution, and similar to Fig. 9 the small crosses represent the statistical-model results for the three specific neutron multiplicities.

tions, the TKE dependence of M_n^{pre} might be a signature of such noncompound fission contributions, even if there is no evidence in fragment mass and angular distributions. A similar M_n^{pre}–TKE relation was observed for systems where fast-fission components are expected: ^{165}Ho,^{238}U+^{40}Ar (249 MeV) (Ref. 51), and for ^{232}Th+^{20}Ne (214 MeV) (Ref. 2) (though the effect here was not emphasized due to poor energy resolution of the fission fragment detectors).

Another possible interpretation[52] for the TKE dependence of pre-scission neutron emission could be that different paths of the fissioning nucleus from saddle to scission might consume different amounts of energy in collective motion. When plenty of energy is available for this motion, the nucleus can "overstretch" and form extraordinary long pre-scission shapes and low TKE values. Pre-scission neutrons remove energy, and hence events with extremely low kinetic energy and high post-scission multiplicity are strongly suppressed. In addition, the temperature parameters T^{pre} of the pre-scission neutron component (see Table III) indicate, though with large errors, that low TKE values are correlated with high excitation energies.

V. SUMMARY

Pre- and post-scission neutron multiplicities were measured for different fission fragment masses and TKE bins of the fusion-fission reaction ^{169}Tm(^{36}Ar,f) at E_{lab}=205 MeV. The observed spread in fragment mass and TKE distributions is consistent with values found in systems with similar fissility and excitation energy. The primary mass width σ_A=18.7 is broader by 20% than the statistical-model prediction and, according to systematics,[8,14] is consistent with the assumption of a fusion-fission reaction. The width of the out-of-plane fragment correlation angle is mainly due to particle evaporation and depends on the mean kinetic energy of the emitted particles. This width could be reproduced by evaporation calculations. The neutron deficient compound nucleus ^{205}Fr on the average evaporates only 1.2±0.5 neutrons before scission leaving each symmetric fission fragment at relatively high excitation energy of ≈40 MeV. A large ratio of post-scission to pre-scission neutrons favors the determination of temperature parameter T^{post} and multiplicity M_n^{post} in a multiple-source fitting procedure. Nevertheless the experimental accuracy was not sufficient to determine the level-density parameter unambiguously from the shape of the neutron spectra and the width of the out-of-plane fission fragment correlation angle.

The fragment mass dependence of the post-scission neutron multiplicity could be well described by the statistical model assuming that the energy at scission is split between the fragments in proportion to their mass. From the measured average pre-scission neutron multiplicity a fission decay time in the range of 10^{-20}–10^{-19} s could be deduced, depending on the level-density parameter used. Long reaction times are finger prints of large-scale collective nuclear motions, and a reliable determination of the level-density parameter would enable the classification of this collective motion into "fast" and "slow" processes.

No fragment mass split dependence of the pre-scission neutron multiplicity was observed. However, for the first time clear experimental evidence is seen of an increased pre-scission neutron multiplicity with increasing TKE of the fission fragment. This unexpected behavior might either reflect a characteristic feature of heavy-ion-induced fusion-fission reactions, where composite systems with high excitation energies are produced, or might be evidence for noncompound fission reactions, indicating faster reaction times for trajectories where more elongated shapes of the composite system are formed.

At this stage of our understanding an unequivocal interpretation of the relation between the pre-scission neutron multiplicity and the total kinetic energy of the fragments cannot be presented, but these kinds of measurements seem to be an invaluable tool for the study of fission dynamics. Further experiments are in progress to clarify this novel feature of fission.

ACKNOWLEDGMENTS

We are obliged to U. Brosa for valuable comments and suggestions and for his RNR model calculations of fragment excitation energies at scission for the system analyzed in this work. We would also like to thank W. Scobel for providing us with large-diameter neutron detectors (Bundesministerium für Forschung und Technologie Contract No. 06-HH-175).

[1]D. Hilscher, H. Rossner, B. Cramer, B. Gebauer, U. Jahnke, M. Lehmann, E. Schwinn, M. Wilpert, Th. Wilpert, H. Frobeen, E. Mordhorst, and W. Scobel, Phys. Rev. Lett. **62**, 1099 (1989).

[2]D. J. Hinde, H. Ogata, M. Tanaka, T. Shimoda, N. Takahashi, A. Shinohara, S. Wakamatsu, K. Katori, H. Okamura, Phys. Rev. C **39**, 2268 (1989).

[3]A. Gavron, A. Gayer, J. Boissevain, H. C. Britt, T. C. Awes, J. R. Beene, B. Cheynis, D. Drain, R. L. Ferguson, F. E. Obenshain, F. Plasil, G. R. Young, G. A. Petitt, and C. Butler, Phys. Rev. C **35**, 579 (1987).

[4]W. P. Zank, D. Hilscher, G. Ingold, U. Jahnke, M. Lehmann, and H. Rossner, Phys. Rev. C **33**, 519 (1986).

[5]C. Riedel, G. Wolschin, and W. Nörenberg, Z. Phys. A **290**, 47 (1979).

[6]P. Fröbrich and J. Stroth, in XVIIth International Winter Meeting on Nuclear Physics, Bormio, 1989 (unpublished).

[7]J. Stroth *et al.*, Ric. Sci. Educ. Perm. Suppl. **63**, 659 (1988).

[8]W. Q. Shen, J. Albinski, A. Gobbi, S. Gralla, K. D. Hildenbrand, N. Herrmann, J. Kuzminski, W. F. J. Müller, H. Stelzer, J. Tōke, B. B. Back, S. Bjørnholm, and S. P. Sørensen, Phys. Rev. C **36**, 115 (1987).

[9]T. Døssing and J. Randrup, Nucl. Phys. **A433**, 215 (1985).

[10]A. J. Sierk, Phys. Rev. C **33**, 2039 (1986).

[11]H. Rossner, J. Erxmeyer, D. Hilscher, and M. Lehmann, in *Proceedings of the Symposium on Heavy Ion Interactions Around the Coulomb Barrier, Legnaro, Italy, 1988,* Vol. 317 of *Lecture Notes in Physics,* edited by C. Signorini, S. Skorka, P. Spolaore, and A. Vitturi (Springer, Berlin, 1988), p. 167.

[12]L. C. Vaz and J. M. Alexander, Phys. Rep. **97**, 1 (1983).

[13]J. P. Blocki, H. Feldmeier, and W. J. Swiatecki, Nucl. Phys. **A459**, 145 (1986).

[14]B. Borderie, M. Berlanger, D. Gardès, F. Hanappe, L. Nowicki, J. Péter, B. Tamain, S. Agarwal, J. Girard, C. Grégoire, J. Matuszek, and C. Ngô, Z. Phys. A **299**, 263 (1981).

[15]B. Gebauer, M. Wilpert, Th. Wilpert, Hahn-Meitner-Institut Annual Report 1987 (unpublished).

[16]L. Meyer, Phys. Status Solidi B **44**, 253 (1971).

[17]L. Meyer and P. Krygel, Nucl. Instrum. Methods **98**, 381 (1972).

[18]V. E. Viola, K. Kwiatkowski, and M. Walker, Phys. Rev. C **31**, 1550 (1985).

[19]R. A. Cecil, B. D. Anderson, and R. Madey, Nucl. Instrum. Methods **161**, 439 (1979).

[20]M. Hilman and Y. Eyal (unpublished).

[21]A. Gavron, Phys. Rev. C **21**, 230 (1980).

[22]V. F. Weisskopf, Phys. Rev. **52**, 295 (1937).

[23]J. M. Blatt and V. F. Weisskopf, *Theoretical Nuclear Physics* (Wiley, New York, 1952), p. 367.

[24]D. W. Lang, Nucl. Phys. **77**, 545 (1966).

[25]J. Gilat and J. R. Grover, Phys. Rev. C **3**, 734 (1971).

[26]F. Pühlhofer, Nucl. Phys. **A280**, 267 (1977).

[27]D. Wilmore and P. E. Hodgson, Nucl. Phys. **55**, 673 (1964).

[28]F. G. Perey, Phys. Rev. **131**, 745 (1963).

[29]J. M. Lohr and W. Haeberli, Nucl. Phys. **A232**, 381 (1974).

[30]J. R. Huizenga and G. Igo, Nucl. Phys. **29**, 462 (1962).

[31]D. Hilscher, D. J. Hinde, and H. Rossner, in the XVIIIth International Symposium on Nuclear Physics, Physics and Chemistry of Fission, Gaussig, German Democratic Republic, 1988 (unpublished); D. Hilscher, D. J. Hinde, and H. Rossner, in *Proceedings of the Texas A&M Symposium on Hot Nuclei, College Station, Texas, 1987,* edited by S. Shlomo, R. P. Schmitt, and J. B. Natowitz (World Scientific, Singapore, 1988), p. 193.

[32]K. J. Le Couteur and D. W. Lang, Nucl. Phys. **13**, 32 (1959).

[33]B. E. Watt, Phys. Rev. **87**, 1037 (1952).

[34]C. Budtz-Jørgensen and H.-H. Knitter, Nucl. Phys. **A490**, 307 (1988).

[35]R. Bass, Phys. Rev. Lett. **39**, 265 (1977).

[36]D. Hilscher, J. R. Birkelund, A. D. Hoover, W. U. Schröder, W. W. Wilcke, J. R. Huizenga, A. C. Mignerey, K. L. Wolf, H. F. Breuer, and V. E. Viola, Jr., Phys. Rev. C **20**, 576 (1979).

[37]E. Holub, D. Hilscher, G. Ingold, U. Jahnke, H. Orf, and H. Rossner, Phys. Rev. C **28**, 252 (1983).

[38]S. Kapoor, R. Ramanua, and R. Rama Rao, Phys. Rev. **131**, 283 (1963).

[39]V. P. Éismont, At. Energ. **19**, 113 (1965) [Sov. At. Energ. **19**, 1000 (1965)].

[40]E. Cheifetz, Z. Fraenkel, J. Galin, M. Lefort, J. Péter, and X. Tarrago, Phys. Rev. C **2**, 256 (1970).

[41]T. Sikkeland and V. E. Viola, in *Proceedings of the Third Conference on Reactions Between Complex Nuclei, Asilomar, 1963,* edited by A. Ghiorso, R. M. Diamond, and H. E. Conzett (University of California Press, Berkeley, 1963), p. 232.

[42]R. Bock, Y. T. Chu, M. Dakowski, A. Gobbi, E. Grosse, A. Olmi, H. Sann, D. Schwalm, U. Lynen, W. Müller, S. Bjørnholm, E. Esbensen, W. Wölfi, and E. Morenzoni, Nucl. Phys. **A388**, 334 (1982).

[43]V. E. Viola, Jr. and T. Sikkeland, Phys. Rev. **130**, 2044 (1963).

[44]Yu. A. Lazarev, in *Proceedings of the EPS Topical Conference on Large Amplitude Collective Nuclear Motions, Keszthely, Hungary, 1979,* edited by Á. Kiss, J. Németh, and J. Zimányi, (Central Research Institute for Physics, Budapest, 1979), Vol. I, p. 244.

[45]U. Brosa and S. Grossmann, J. Phys. G **10**, 933 (1984).

[46]S. Grossmann, U. Brosa, and A. Müller, Nucl. Phys. **A481**, 340 (1988).

[47]Z. Fraenkel, I. Mayk, J. P. Unik, A. J. Gorski, and W. D. Loveland, Phys. Rev. C **12**, 1809 (1975).

[48]D. J. Hinde, J. R. Leigh, J. J. M. Bokhorst, J. O. Newton, R. L. Walsh, and J. W. Boldeman, Nucl. Phys. **A472**, 318 (1987).

[49]H. Rossner, J. R. Huizenga, and W. U. Schröder, Phys. Rev. C **33**, 560 (1986).

[50]U. Brosa and S. Grossmann, Z. Phys. A **310**, 177 (1983).

[51]D. J. Hinde, D. Hilscher, and H. Rossner, in Proceedings of the International Conference on Fifty Years Research in Nuclear Fission, Berlin, 1989, edited by D. Hilscher, H. J. Krappe, and W. von Oertzen [Nucl. Phys. (to be published)].

[52]U. Brosa (private communication).